Rotation Sensing Using Passive RFID Tags

Swadhin Pradhan
UT Austin, USA

Shuozhe Li
UT Austin, USA

Lili Qiu
UT Austin, USA

ABSTRACT

Rotational movement is important in many applications, yet has been under-explored. In this paper, we explore the feasibility of using a single RFID reader antenna to simultaneously sense rotation and translation movement (*i.e.*, rotation axis, rotation speed, and translation speed). We exploit the polarization in RFID to enable motion sensing. We develop an analytical model to capture the impact of polarization on the received signal and an optimization framework to incorporate the model to estimate the movement. We implement our system, Tag-based Inertial Measurement Unit (*TIMU*), and demonstrate its effectiveness through an extensive evaluation. To our knowledge, this is the first system that tracks general motion using a single RFID reader antenna.

CCS CONCEPTS

• **Human-centered computing** → *Ubiquitous and mobile computing design and evaluation methods.*

KEYWORDS

Passive RFID, Polarization, Rotation sensing.

1 INTRODUCTION

Recently there has been a surge of research interest in motion sensing. Many innovative sensing approaches have been proposed using a variety of wireless signals, including WiFi (*e.g.*, [12], acoustic (*e.g.*, [28]), RFID (*e.g.*, [26, 34]), and 60 GHz (*e.g.*, [35]). Most of these works estimate distance and angle of arrival to track translation.

Interestingly, rotation tracking is under-explored. On the other hand, rotation plays a significant role in many applications (*e.g.*, sports analytics, factory assembly line monitoring). Moreover, existing device-free motion tracking systems, including WiFi, acoustic, laser, do not track the ball movement well due to its small size, which limits the amount of reflection and results in a large error.

Gyroscope based approach is one way to sense rotational movement, however, gyroscope gets saturated within a few revolutions per second [7]. To improve accuracy, [16] combines gyroscope with
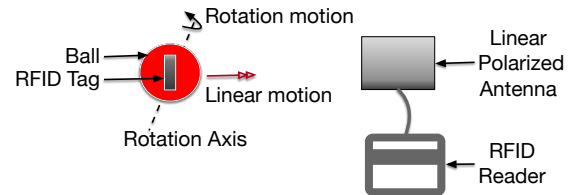
Figure 1: Architectural Overview of TIMU.

magnetometer and UWB beacon with an antenna array to track a ball's rotation. However, it requires battery and significant modification to the ball. Battery replacement is not only costly but also inconvenient. Moreover, the gyroscope, magnetometer, and UWB should be placed carefully inside a ball to track its rotation. This significantly increases the manufacturing cost and the weight of the ball, which is undesirable. It also requires a way to communicate the sensed motion from the ball back to the analytics system.

Long-range high-resolution camera network is another option but suffers from occlusion and high cost ($100,000+) [16]. It is not good at tracking fast rotation (*e.g.*, beyond 50 RPM) even with clear markers. Tagyro [36] places multiple parallel tags on an object and tracks the phase change to estimate the 3D orientation. Therefore [36] requires tags with a large separation (*e.g.*, 8.2 cm), multiple antennas, and extensive calibration.

Our approach: Motivated by the existing works and their limitations, we propose a novel translation and rotation tracking algorithm using a *single* RFID reader antenna. A reader with a single antenna is much cheaper and more readily available. Our tracking system can achieve (i) high tracking accuracy for both rotation and translation movement, (ii) low cost (because of single port RFID reader with a single antenna costs $600 compared to multi-port RFID reader with four antennas cost around $3000), (iii) easily customizable for different shapes and sizes, (iv) negligible physical foot-print, and (v) battery-free. It is a passive battery-free sensing approach using RFID. We attach RFID tags to a ball and use a commercial-off-the-shelf (COTS) reader to sense both rotation and translation movement as shown in Figure 1, where the tag and reader antenna are both linearly polarized to enable accurate battery-free motion sensing. Our system is user friendly since RFID tags are cheap, light-weight, and easy to attach. We exploit the polarization between an RFID tag and a reader antenna for tracking using a *single* reader antenna. Due to RFID polarization, the magnitude and phase of the received signal are significantly affected by the relative orientation and position between the RFID antenna and tag. Therefore, we can use the reflected signal arriving at the RFID antenna to estimate the motion.

To maximize the accuracy, we use a linearly polarized tag and reader antenna, since the received signal in this case is most sensitive to the relative orientation and position between the tag and reader antenna. Moreover, linear polarization also significantly reduces the multipath since signals outside the polarized direction are significantly weakened.

To realize this vision, we decompose the general tracking problem into three more tractable sub-problems: (i) tracking rotation given a fixed ball position, (ii) tracking translation movement, and (iii) integrate the rotation tracking and translation tracking.

For (i), we analytically derive the reflected signal arriving at the RFID antenna given the relative position and orientation between the reader and tag by considering the polarization and non-uniform gains of the RFID reader and tags. We apply our model to derive the received signals during rotation for a given rotation axis. We then search the rotation axis whose estimated signals during a rotation best matches with the measurement. We cast this tracking problem as a non-convex optimization problem and design a deep neural network (DNN) to efficiently find a good initial solution. We further refine the solution by capturing the temporal locality.

For (ii), we use the phase change to track the relative distance change and use frequency hopping to get the absolute distance. Tracking the angle of arrival (AoA) using a single antenna is more challenging. Existing works require multiple antennas to estimate AoA. We realize one-antenna based AoA estimation by using the same non-linear optimization framework, which leverages the polarization and non-uniform gains in the antenna and tags. We *cannot* guarantee a unique RSS pattern across all AoAs and rotation axes, so our scheme to determine AoA and rotation axis simultaneously is *best effort*. Its accuracy improves by using multiple tags with different orientations and leveraging temporal locality during movement.

Finally, we integrate our rotation tracking with translation tracking to handle general movement involving both rotation and translation. We build a system, called TIMU (Tag Inertial Measurement Unit), which turns COTS RFID Tags into battery-free IMUs. It measures motion parameters, including rotation axis, rotation speed, 3D position in a battery-free manner, while eliminating the need for an additional communication channel to report.

Our contributions can be summarized as follow: (i) We develop a systematic model that captures the impact of polarization between an RFID tag and a reader antenna on the phase and magnitude of the received signal. It captures non-uniform gain between the RFID tags and reader antenna. (ii) We design a novel algorithm that uses the polarization to estimate the rotation axis and average rotation speed using a *single* RFID reader antenna. We extend our algorithm to further estimate AoA as well as distance using a *single* RFID reader antenna. To the best of our knowledge, this is the *first* system that senses general motion including both rotation and translation using a single RFID reader antenna. (iii) We implement and evaluate our approach and demonstrate its feasibility in a range of scenarios, including environments with static or dynamic multipath.

2 RELATED WORKS

There have been significant research on motion tracking. We group them based on the type of signals being used.

IMU: Researchers in [17] embed IMUs in a cricket ball to extract relevant features, such as angular velocity, time of flight, ranging. Moreover, [21] measures spin-analytics in the context of a bowling ball. However, the tracking accuracy degrades significantly as the rotation speed increases. It is also challenging to track moving distance using inertial sensors due to error accumulation [20].

Wireless tracking: There has been lots of wireless tracking effort during the past decades. Many existing works employ different channel characteristics for tracking, such as Angle of Arrival (AoA) [22], Time of Flight (ToF) [15], and channel state information (CSI), or their combination [38]. [23] pushes the accuracy to sub-centimeter level. These approaches, however, usually require a large phased array, a large frequency bandwidth, and Line-Of-Sight (LOS) condition to achieve good performance.

System	Goal	Key Innovation	Limitation
TTrack [24]	Fine-grained single-shot 3D tag tracking	Large bandwidth (100 MHz) and OFDM	Three USRPs with six antenna setup with off-line Gaussian HMM based tracking
RFind [25]	Fine-grained tag tracking	Large bandwidth (300 MHz) + multi-antennas	Custom USRP setup with off-line clustering based tracking
RFComp. [33]	Robot object manipulation	use SAR to build multi-path profile	Coarse-grained tracking possible
PDraw [31]	Tag movement tracking	Use the effect of orientation of passive tag on back-scattered signal	Recognize a fixed set of alphabets using a two antenna based setup
Tagyro [36]	Estimate static 3D orientation	Use phase change at multi-antennas	Extensive initial calibration
OmniTrack [19]	Estimate static 3D orientation and location	Use polarization at multi-antennas	Extensive initial calibration

Table 1: Summary of a few RFID based tracking systems.

RFID-based tracking: Passive RFID based sensing is closely related to our work. We summarize various schemes in Table 1. Among them, Tagyro [36] tracks rotation movement. It tracks the 3D orientation of a passive object using two orthogonal RFID reader antennas and an array of passive RFID tags. Our work advances [36] in the following ways: (i) [36] requires multiple reader antennas whereas we show the feasibility of general motion tracking using a single reader antenna, (ii) we exploit polarization and non-uniform gain values in the RFID reader and tags to achieve higher resolution whereas Tagyro [36] only considers the impact of distance on the phase, and (iii) we track general motion involving both rotation and translation movement while [36] only tracks rotation.

Moreover, [19] tracks the 3D location and orientation of an object using the polarization property of passive RFID tags. Our work differs from [19] in several important aspects: i) we track an object motion using *a single* reader antenna while [19] requires multiple circularly polarized antennas, ii) we track both rotation and translation movement while [19] tracks the position and orientation of a static object and requires more fine-grained initial calibration, higher bandwidth, and more antennas, iii) we develop an analytical model to enable rotation tracking without absolute localization.

[32] develops an interesting technique to improve RFID range. Our work is orthogonal to improving RFID range, and can directly benefit from other RFID systems with increased range.

3 MODEL FOR RFID SIGNAL

We develop a model to capture the impact of relative orientation of the RFID reader and tag on the received signal due to polarization. We borrow from existing literature to provide a general framework.

3.1 Model of Received Signal Phase

We first examine how the movement affects the phase of the received signal. Let r denote the distance between the reader antenna and tag. The signal traverses a total distance of $2r$ due to back scattering. The received phase is determined by both the distance and additional phase offsets introduced by the transmitter, tag, and receiver circuits, denoted as θ_T, θ_{TAG} and θ_R, respectively. The total phase change [2] at the reader is $\theta = (\frac{2\pi}{\lambda} \times 2r + \theta_T + \theta_{TAG} + \theta_R)\ mod\ 2\pi$ where λ is the wavelength. $\theta_T + \theta_R$ can be expressed as polarization mismatch $2\phi(\hat{r})$ or 2γ. θ_{TAG} can be expressed as $arg(\frac{1}{Z_A+Z_C(OFF)} - \frac{1}{Z_A+Z_C(ON)})$. If we assume $Z_C(OFF) \rightarrow \infty$ (i.e., practically very large) [14, 27], it becomes $\theta = (\frac{2\pi}{\lambda} \times 2r + 2\gamma + arg(-\frac{1}{Z_A+Z_C(ON)}))\ mod\ 2\pi$.

If we measure frequently enough without phase wrap-around, $\theta = \frac{2\pi}{\lambda} \times 2r + 2\gamma + C$, where $C = arg(-\frac{1}{Z_A+Z_C(ON)})$ is a constant. γ is the polarization mismatch angle between the reader and tag antennas. For a linearly polarized RFID reader antenna and tag directly facing each other (e.g., azimuth angle = 0), γ equals the relative orientation (e.g., $\gamma = 0$ when they are in parallel and $\gamma = \pi/2$ when they are orthogonal). When the azimuth is non-zero, γ is the sum of the relative orientation and azimuth [30, 31].

3.2 Received Signal Strength

Let the RFID reader antenna transmit at power P_t. The transmission power density D_t [13, 18] of the tag at a distance r is: $D_t(\theta_t, \phi_t) = \frac{P_t G_t(\theta_t, \phi_t)}{4\pi r^2}$ where $G_t(\theta_t, \phi_t)$ is the directional gain of the reader antenna, and θ_t and ϕ_t are polar measures in the reader antenna's coordinate system. The tag antenna's intercepted power from this dissipation is: $P_{tag} = D_t(\theta_t, \phi_t)A_e$, where A_e is the effective area of the tag antenna and expressed by $\frac{G_{tag}(\hat{\theta}_t, \hat{\phi}_t)\rho\lambda^2}{4\pi}$, $G_{tag}(\hat{\theta}_t, \hat{\phi}_t)$ is the directional gain of the tag antenna, λ is the wavelength of the reader's signal, and ρ is the polarization loss factor, i.e, a function of polarization mismatch between the reader and tag antennas.

When both the reader and tag antenna are linearly polarized, the polarization loss factor (ρ) can be expressed as $\rho = cos^2(\gamma)$, where γ is the polarization mismatch between the two antennas. Using the free-space model, we get the received power (P_{rec}) as follows [13, 18]:

$$P_{rec} = P_t G_t(\theta_t, \phi_t)^2 G_{tag}(\hat{\theta}_t, \hat{\phi}_t)^2 K cos^4(\gamma)(\frac{\lambda}{4\pi r})^4 \qquad (1)$$

where K is the modulation loss of the tag antenna (the value is less than 1) and depends on the impedance matching between the chip and tag antenna. This indicates that

$$P_{rec} \propto P_t G_t^2 G_{tag}^2 r^{-4} K cos^4(\gamma)\frac{1}{r^4} \qquad (2)$$

To use our model, we derive the gain values of the tag and reader antennas based on their relative geometric positions for each position according to their data sheets.

3.3 Model Validation

Measured vs. modeled phase and RSS: We compare the model with measurement from our RFID setup. Fig. 2 show the measured and modeled phase during a rotation when the ball is rotating around the following rotation axes: (0,0,30), (45, 0, 20), and (0, 60,

60). Figure 3 compares the measured and modeled RSS under the same rotation axes. As we can see, different rotation axes tend to have different phase and RSS patterns. This suggests that it is potentially feasible to use the phase and RSS patterns to estimate how the ball rotates. Moreover, our modeled phase and RSS closely follow the measurement.
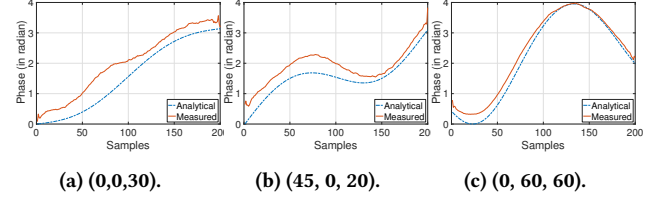

| (a) (0,0,30). | (b) (45, 0, 20). | (c) (0, 60, 60). |

Figure 2: Validation of Phase with different Rotation Axis Configurations (Yaw, Pitch, Roll).

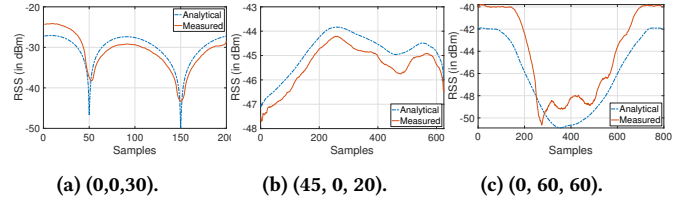| (a) (0,0,30). | (b) (45, 0, 20). | (c) (0, 60, 60). |

Figure 3: Validation of RSS with different Rotation Axis Configurations (Yaw, Pitch, Roll).

Modeling error: We further quantify the accuracy of our model by collecting received signals over 200 different rotation axes at a 0.5m distance. We rotate the balls at least 5 times, and automatically detect the start and end of the rotation as described in Sec. 4.1. We align the measurement samples across different rotations using correlation and compute the median across all rotations for each sample. We compute the average difference between the samples from our measurement with those from our model. The median phase error is 0.1 radian and the median RSS error is 3 dBm.

Impact of multipath: We evaluate the impact of multipath by collecting additional measurements in two ways: one without intentionally adding multipath and one with intentionally adding multipath by placing 5 wooden reflectors ($1m \times 1m$ large and $1cm$ thick) wrapped with aluminum foil near the LoS path between the tag and the reader antenna. Two reflectors are placed on each side of the line connecting the tag and reader antenna and one reflector is placed behind the tag. The two configurations differ in their angles intersecting the line between the tag and reader antenna. Fig. 4(a) and Fig. 4(b) compare the modeled and measured phase and RSS. As we can see, the modeled RSS and phase match well with the measurement. The match is close even under multipath since linearly polarized tags and reader antenna significantly weaken the signals coming in other directions and limit multipath.

We also create dynamic multi-path situations: (i) by moving a wooden barrier (1 m × 1m large, 5 cm thick) around intermittently blocking the direct path between the tag and antenna, and (ii) by moving the wood but avoid blocking the direct path between the tag and antenna. Fig. 4(c) and Fig. 4(d) show that there is distortion in the blocking scenario but the overall shapes remain similar.
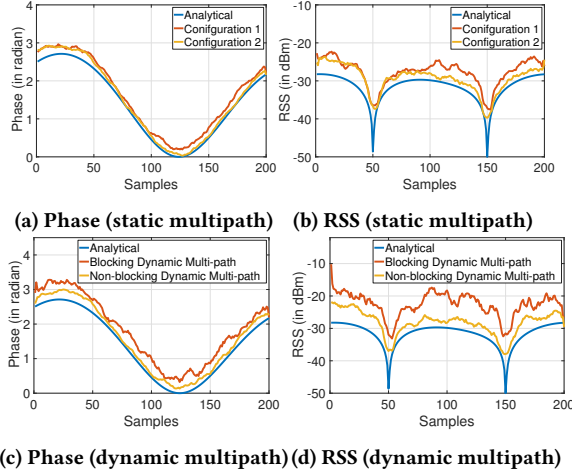
(a) Phase (static multipath) **(b) RSS (static multipath)**

(c) Phase (dynamic multipath) **(d) RSS (dynamic multipath)**

Figure 4: Measured vs. modeled phase and RSS under static and dynamic multipath along the rotation axis (70,30,15).

4 TRACKING ALGORITHM

To track a ball, we attach multiple RFID tags to the ball. We develop a tracking algorithm to estimate its translation and rotation movement incrementally. For simplicity, in this paper we assume an integer number of rotations. First, we consider the ball's position is fixed and known, and design an algorithm to estimate its rotation axis and speed. Then we relax the assumption and estimate the ball's position in addition to its rotation axis and speed.

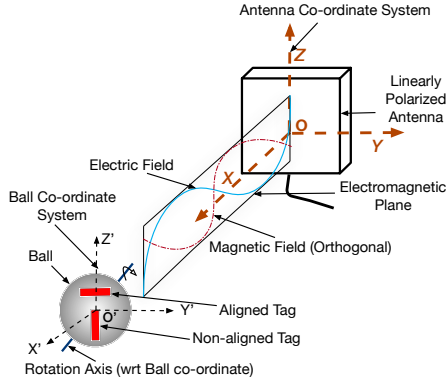## 4.1 Estimate Rotation Axis and Speed

Figure 5: Polarization and coordinate Systems of TIMU.

We use the setup shown in Fig. 5. We calculate the rotation axis with respect to the ball's coordinate system. We set the center of the RFID antenna as the origin. We transform the ball coordinate using proper rotation matrix multiplication and translation transformation. The azimuth defines the horizontal angle between the ball and reader antenna, and the elevation defines the vertical angle between the ball and reader antenna. We choose linear polarized reader and tag antennas (i.e., the electric magnetic field is confined to a plane as shown in Fig. 5) since it results in deterministic and distinguishable phase and RSS patterns during rotation. Furthermore, as shown

in Fig. 5, we place multiple tags with different orientations with respect to the polarization plane of the RFID reader antenna to maximize diversity.

4.1.1 Estimate Rotation Axis. First, we consider how to estimate the rotation axis. We observe different rotation axes result in different RSS and phase patterns during a rotation. Therefore we can use the RSS and phase measurements from a rotation to infer the rotation axis. In particular, we leverage the model in Section 3.

Problem formulation: Our goal is to search for the rotation axis $(\theta_1, \theta_2, \theta_3)$ such that the resulting received signals best matches the measured signals. We detect the start and end of a rotation based on the periodic RSS pattern as described in Sec. 4.1.2. Let r_k^i denote the i-th measured received signal from tag k during one rotation, N denote the total number of samples we get from each tag in one rotation, and M denote the total number of tags.

Given the ball size, position, rotation axis, and the number of samples per rotation, we can derive the tag trajectory during a rotation based on geometry. We uniformly sample the trajectory. We need enough samples per rotation in order to get a detailed RSS trace for estimating the rotation axis. We empirically evaluate the impact of the number of samples per rotation on estimation accuracy. For each position on the trajectory, we compute its phase and RSS as described in Section 3 to get a complex signal. Let $m_k^i(\theta_1, \theta_2, \theta_3)$ denote the i-th received complex signal from tag k during the rotation estimated using our model when the rotation axis is $(\theta_1, \theta_2, \theta_3)$. Our goal is to search for the rotation axis that minimizes the fitting error with the measured signals across tags:

$$min_{\theta_1, \theta_2, \theta_3} \sum_k |m_k^i(\theta_1, \theta_2, \theta_3) - r_k^i| \qquad (3)$$

Signal alignment: This formulation assumes the modeled and measured signals are properly synchronized. This is achieved by computing the correlation between the two signals at all offsets and finding the offset that yields a peak in the correlation.

Algorithm: The problem is challenging to solve since the objective is non-convex and has many local optimals. One option is to perform binary search or hierarchical search. But it does not work well since a local optimal may be surrounded by points that are far away from the optimal. Another option is to generate profiles for all possible rotation axes at a given granularity using our model and exhaustively compare the measurement against all profiles from our model. But this is expensive. If we resort to a coarse search resolution to speed up the search, the accuracy would degrade. Instead, we formulate non-convex optimization and use fmincons() in matlab to solve it. It is challenging to get a global optimal solution. The optimization results are sensitive to the initialization. In order to get a good solution, we need an initial solution that is not too far away from the optimal.

To improve the speed and quality of the search, we develop two strategies. First, we use a machine learning algorithm to find an initial solution. We use deep neural network (DNN) as the machine learning algorithm. The advantage of using a DNN is that it can approximate any function with arbitrary accuracy. We use a fully connected 4-layer DNN, which has 600, 500, 400, and 300 neurons at the first, second, third, and fourth layers respectively. The DNN maps the phase and RSS samples during one rotation to the 3D
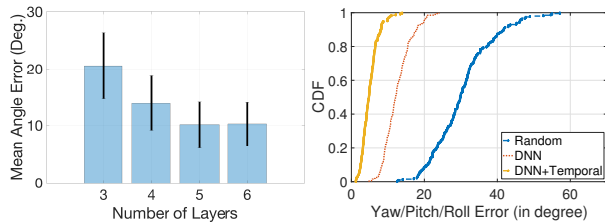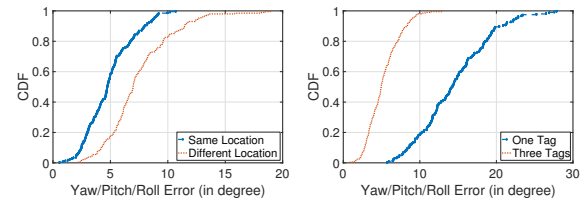
Figure 6: (a) Empirical Parameter Selection of a fully-connected DNN for initialization. (b) CDF of Error using different initialization.

(a) CDF of Error using training (b) CDF of rotation axis error and testing from two locations. ror using 1 or 3 tags.

Figure 7: Yaw/Pitch/Roll Error (in degree).

(a) Example of RSS during (b) Rotation Clock-wise or two complete rotations. Reverse Clock-wise.

Figure 8: Example Patterns of RSS and Phase.

rotation axis. Following the common practice, we normalize the inputs using 'ReLu' transfer function for hidden layers, and finish with a single unit with a 'sigmoid' activation. The neural network is trained using Adam optimizer, the learning rate of 0.0000001, and the maximum iterations of 100000. We generate the training data using a combination of measurement data and synthetic data derived from our model. Our results show that the initial solution derived from the DNN significantly improves the solution quality and search speed. To finalize a specific architecture, we have tried several other configurations. Fig. 6(a) shows the average error reduces initially as we increase the number of layers from 3 to 5, and then tapers off.

To further improve the accuracy, instead of searching for a rotation axis independently for each rotation, we further leverage the temporal locality between consecutive rotations by generating multiple initial solutions from injecting a small random noise to the output from DNNs and feeding each of the perturbed initialization to $fmincons$ in Matlab. In this way, we obtain L candidate solutions for each rotation. We select the candidate solution from each rotation to minimize the total difference between the consecutive rotation axes to capture the temporal locality. To achieve this goal, we construct a graph with $L \times R$ nodes (L nodes per rotation and R rotations). We fully connect the nodes in rotation i with those in rotation $i + 1$ with edge weights that represent the Euclidean distance between their corresponding rotation axes. We find the shortest path in the graph. The solutions to the nodes on the shortest path are the final rotation axes. Our evaluation shows that $L = 5$ and $R = 3$ give good balance between the computation cost and accuracy.
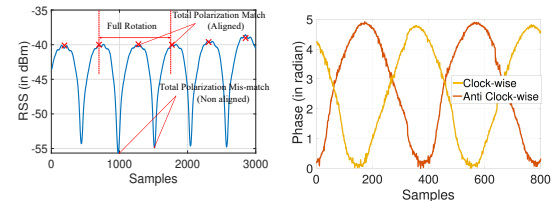
Figure 6(b) shows the CDF of estimation errors using random initialization, DNN, and DNN with temporal locality. As we can see, the median error decreases from 32.5 degree in random initialization to 9 degrees in DNN and to 5 degrees in DNN with temporal locality. Furthermore, to observe the dependence of data collection setup in our DNN initialization, we collect rotation axes data in two locations. We use one for training and the other for estimating and vice versa. As shown in Fig. 7a, If we use data from the same location compared to different locations in training vs estimating, the median error for angular estimation goes from 5.5 degree to 7.5 degree, as illustrated in Fig. 7a. The error does not increase significantly because the pattern remains similar for a certain rotation axis due to the polarization property.

Multiple tags: This optimization can support multiple tags by summing up the fitting errors across all tags. This helps to avoid

the zones that have similar rotation templates and reduce error. To balance the computation cost and accuracy, we use 3 tags. Fig. 7b shows that using three tags can reduce the median estimation error of the rotation axis from 15 degree to 5 degree.

We use a Macbook Pro running OS Sierra with a 8GB RAM, and i5 quad-core processor to process the data. It takes on average around 0.5 second to run the DNN based initialization and 1.5 seconds to estimate the parameters of rotation with other related values.

4.1.2 Estimate Rotation Speed. As shown in Figure 8a, the received signal strength (RSS) exhibits a periodic pattern as the ball rotates. The RSS reaches a peak when the tag is parallel to the reader antenna (*e.g.*, their angles are at 0°, 180°, 360°). The RSS reaches a valley when the tag and reader antenna are perpendicular to each other. By counting the number of peaks (or valleys), we can estimate the number of rotations per minute (RPM).

4.1.3 Estimate Rotation Direction. Rotation can happen clock-wise or counter-clockwise. For a given ball rotation axis and position, these opposite rotations produce reverse templates as shown in Fig. 8b. Therefore, given the starting position, we can analyze the template pattern to infer the rotation direction.

4.2 Estimate Position Using a Single Antenna

In this section, we focus on estimating the ball position using a single antenna (*i.e.*, the angle of arrival (AoA) and distance from the ball). Our AoA estimation requires the ball to rotate whereas the distance tracking assumes the overall phase change is dominated by the translation movement since we assume an integer number of rotations. We will further integrate rotation and translation tracking in Section 4.3.

4.2.1 Estimate AoA. **Our algorithm:** Existing approaches use an antenna array to estimate the angle of arrival (AoA). We explore

the feasibility of using a single RFID reader antenna to estimate the AoA by exploiting the polarization and non-uniform gains of the reader antenna and tag. We observe that AoA affects the phase and RSS pattern during one rotation, therefore it is possible to use the phase and RSS measurements in a rotation to infer the AoA along with the rotation axis. We apply the same optimization framework in Section 4.1 except that we now add two new unknowns: azimuth and elevation. To improve the search for the rotation axis and AoA, we use another DNN with the same structure as in Section 4.1 except that it has a 5-dimension output vector, which includes the rotation axis, azimuth and elevation. As before, we find DNN based initialization works much better than random initialization since it uses the RSS and phase patterns to determine a good starting point.

The phase and RSS pattern during a rotation is *not* unique across all possible AoAs and rotation axes. Therefore our scheme is *best effort* and its performance improves as we use multiple tags with different orientations and leverage temporal locality between consecutive rotations during matching.
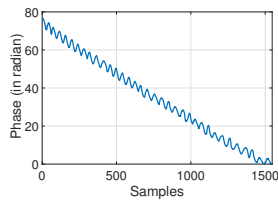

Figure 9: An example phase pattern of a ball with fast rotation and slow translation movement.

4.2.2 Estimate Distance. We use the phase of the received signal to estimate the distance. According to the previous phase model, $\theta = \frac{2\pi}{\lambda} \times 2r + 2\gamma + C$. So we estimate the change in the distance r based on the change in the phase θ. However, due to the phase wrap-around, it only gives the relative distance change. In order to estimate the absolute distance, we use multiple frequencies since they significantly increase the wrap-around period due to Chinese Remainder Theorem [37], which states that solution is unique modulo to Least Common Multiple (LCM) of $\lambda_1, \lambda_2, ..., \lambda_n$ (which is much larger than a single frequency), where n is the number of frequencies. We use two frequencies: 865.7MHz and 867.5MHz, which yields a wrap around period of around 250 ns. This corresponds to around 75 m one way, which is large enough to avoid ambiguity in our context. There is a random phase offset at the reader antenna. To remove the random offset, following [29], we attach an auxiliary tag to the RFID antenna and compute the difference between the phase obtained from the target tag and auxiliary tag. We use the phase difference between the two for distance estimation.

In practice, the commercial RFID reader can only transmit on one frequency at a time. So it performs frequency hopping and uses the two closest samples collected from the two frequencies to derive the absolute distance. The only difference is that we should compensate for the phase change arising from the samples collected at different time. Since we can easily derive the phase change between the previous two samples, we can use it to compensate for the phase change due to different sampling time.

4.3 Supporting Simultaneous Rotation and Translation

Next we study how to estimate both rotation and translation movement at the same time. We observe that the total phase change is the sum of the phase change due to rotation and translation movement. As mentioned earlier, we assume an integer number of rotations, and do not need to compensate the phase change caused by rotation. We remove the impact of the translation movement on the phase change and then estimate the rotation axis.

Based on the above observation, we integrate our rotation estimation in Section 4.1 with our translation motion estimation in Section 4.2 to support both translation and rotation movement. Algorithm 1 shows the pseudo code. Steps 1, 2, 5, and 6 are described in Section 4.1 and Steps 3 and 7 are described in Section 4.2. In step 4, we compensate for the phase change from the translation movement by adjusting the phase of the i-th sample during a rotation by the $-\Delta\theta \times i/N$, where N is the number of samples in a rotation and $\Delta\theta$ is the phase change during one rotation, which is caused by the translation movement since a complete rotation at a position should not change the phase. This assumes constant translation movement during a rotation, which is likely to hold in practice since the velocity tends to remain the same during a small time interval.

Algorithm 1 Final algorithm

1: Estimate the rotation speed based on RSS (Section 4.1.2)
2: Estimate the start and end time of each rotation as the consecutive RSS peaks (Section 4.1.2)
3: Estimate the distance change and direction based on the phase change of the received signal (Section 4.2.2)
4: Compensate for the phase change caused by the translation movement
5: Use the phase and RSS time series from each rotation after compensation to estimate the rotation axis, direction and AoA for the rotation (Section 4.1.1 and Section 4.2.1)
6: Estimate rotation direction (Section 4.1.3)

---

5 EVALUATION

In this section, we first describe our evaluation setup and then present the evaluation results.

5.1 Evaluation Setup

To perform controlled movement experiments and quantify the accuracy of our tracking algorithm, we build a setup that allows us to control the rotation axis, rotation speed, translation speed, and direction as shown in Figure 10. In order to collect the ground truth, we use a moving track [8] whose movement can be programmed and controlled via a laptop using USB. The track is 2.5m long and supports a moving speed from 1cm/s to 3m/s. To drive the motion guide, we use a AMC430 controller [10], a motor driver, and a dedicated power source. Furthermore, to support different rotational axis configurations for evaluation, we 3D print a Goniometer [6] as shown in Fig. 11. We place a RFID tag on the ball above the Goniometer. To create rotational motion, we use a Nema 34 motor [11]
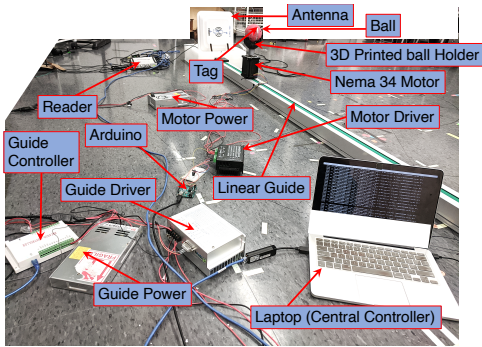
Figure 10: Experimental Setup of TIMU.

with a motor driver and power source [3]. This rotation motion is controlled by Arduino [5], which is in turn connected to the laptop. We vary the translation movement from 1cm/s to 3m/s and rotation speed from 1rpm to 400rpm. Unless otherwise specified, we use a 15cm radius rubber ball in our experiments. We have used a solid rubber ball of 15cm diameter in our experiments which is put at different distances on the track. We also use a wooden cricket ball and plastic ball, and observe similar result since these materials are all non-electromagnetic and have little impact on the RFID tags. The default translation speed, rotation speed, azimuth, elevation, Yaw, Pitch, and Roll values are 10 cm/s, 60 RPM, 20 degree, 20 degree, 0 degree, 0 degree, and 45 degree, respectively. We further vary each of these parameters to understand its impact.

We use a commodity Impinj RFID reader R420 [1], which is ETSI-compliant. It can support frequencies from 865.7MHz to 867.5MHz. We use a 9dBi linearly polarized (RHCP) RFID antenna to leverage its polarization for motion tracking [9], and it is connected to one of the RF ports on the reader. The antenna hops between these two frequencies to estimate the absolute distance. The random phase off-set due to frequency hopping has been resolved using an auxiliary tag as described in [36].We use linearly polarized Alien Squiggle RFID clear wet inlay (ALN-9740) tags [4], which are tuned to work in 840 MHz to 960 Mhz (Global) for our experimental purposes. We use the highest transmission power 32.5dBm. We can achieve a sampling rate of around 200Hz for a single tag and around 50 Hz for three tags in our setup. For 3 tags, we put two tags in parallel 90 degree apart and another tag on the other side in an orthogonal orientation to this tag-pair. Unless otherwise specified, we report the performance of 5 runs for each configuration using error bars or CDFs. The center of the error-bar is the median and its two ends correspond to 25-percentile and 75-percentile. We perform all of the experiments in a typical lab with several furniture (*e.g.*, tables, chairs, desks, shelves) and desktops nearby. To reduce noise in the data, we follow [36] to post-process the phase and RSS measurements by computing the median over a sliding window of 20 samples. The reader sends query reports containing information of ID, RSS, Phase, time-stamp, and channel, via Ethernet to a host laptop. We implement TIMU using RFID library and processing algorithms. We can read these tags with our linearly polarized antenna from up to 10m in line-of-sight setting and up to 6m in non-line-of-sight setting.
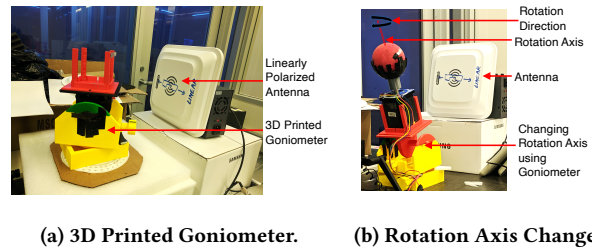

(a) 3D Printed Goniometer.   (b) Rotation Axis Change.

Figure 11: Rotation Setup for TIMU.

5.2 Evaluation Results

We first quantify the tracking accuracy of rotation axis, rotation speed, distance, and AoA estimation. We then evaluate our algorithm under general motion with rotation and translation.

5.2.1 Estimating Rotation. First, we track rotation movement without translation motion. We fix the rotation axis in this experiment and put the ball in a static position. We estimate the number of rotations per minute (RPM) from the peak-counting of RSS patterns.

Estimating rotation speed: We use the periodic RSS change to estimate the rotation speed. Figure 12 plots the rotation speed estimation error as we vary the RPM, distance, rotation axis, and Angle-of-arrival (AoA) (azimuth in this case). As we can see, in all cases we can accurately estimate the rotation speed. Overall, the error increases with the speed and distance as we would expect due to false peak detection.Using an average of 3 tags reduces the RPM error by $20 - 25\%$ due to redundancy.
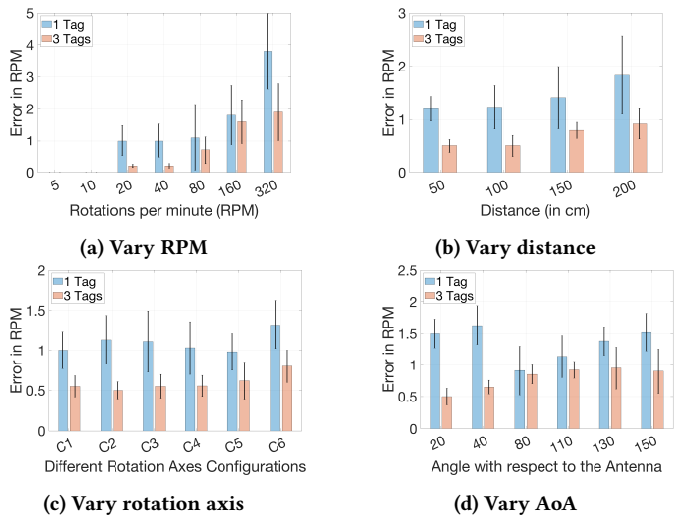

(a) Vary RPM   (b) Vary distance

(c) Vary rotation axis   (d) Vary AoA

Figure 12: Rotation Speed vs RPM error.

Estimating rotation axis: Next, we evaluate the rotation axis estimation (*i.e.*, the relative angle with each of the axes: Yaw (X), Pitch(Y), and Roll(Z)). Figure 13(a) plots the error in estimating the rotation axis as we vary the rotation speed. In this experiment, we create 36 possible configurations by changing X, Y, Z angles using goniometer. As we can see, the errors in the rotation axis are similar as we vary the rotation speed. Figure 13(a) shows that the errors in

the three axes are around 5 degrees in all cases. Figure 13(b) shows that the error increases with the distance due to reduced received signal strength (RSS). Next, we separately vary the azimuth from 20 to 160 degree (20 degree apart), vary the elevation from 10 degree to 70 degree (20 degree apart), and their combinations to generate different 3D positions. As shown in Figure 13(c), the median error is around 5 degrees when we vary only the azimuth or elevation axis. When we vary both, the error increases to 6 degrees.
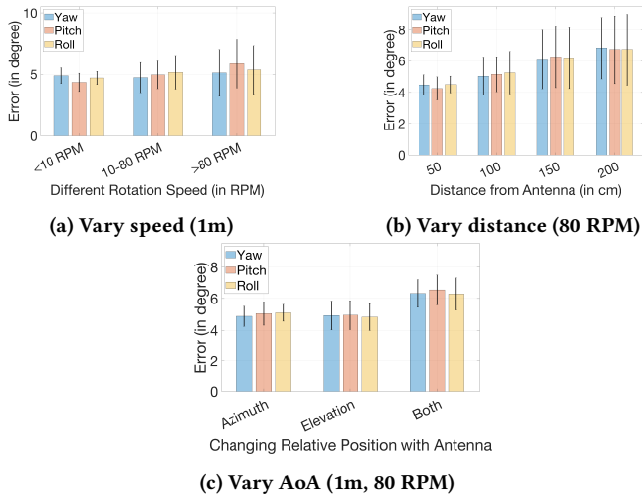

(a) Vary speed (1m)   **(b) Vary distance (80 RPM)**

(c) Vary AoA (1m, 80 RPM)

Figure 13: Rotation axis error with 36 configurations.

5.2.2 Estimating Translation Distance. Next we consider the translation movement without rotation. Figure 14 compares the relative distance change error when we move the ball on the guide with translation movement at different speeds. We calculate the relative distance change using the phase change in one frequency. Fig. 14(a) shows the CDF of the distance estimation error as we vary the speed. It shows the error tends to increase with the speed. Nevertheless, even at a high speed (*e.g.*, over 0.5 m/s), the 90-percentile error is within 2 cm over a 2.5m travel range. Next, we change the azimuth from 20 degree to 150 degree while setting the ball speed at 10 cm/s. Fig. 14(b) shows the impact of azimuth on the distance estimation error is small. Next, we use two frequencies to
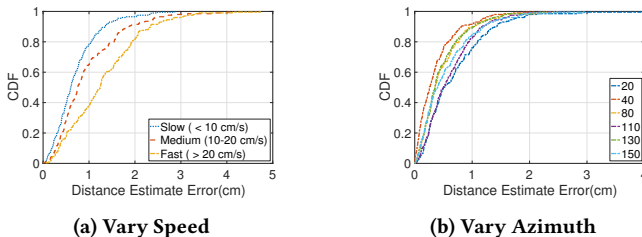

(a) Vary Speed   **(b) Vary Azimuth**

Figure 14: Relative Distance Error using 1 Frequency.

estimate the absolute distance. Figure 15(a) compares the absolute distance error when the ball is stationary, and shows that even at different distances (up to 2m), the 90 percentile error is within 1.5 cm. Note that the duration of data collection should be longer than

the time that takes to get measurements from different frequencies for absolute distance estimation. Figure 15(b) compares the absolute distance error when the ball is moving at different speeds. As we can see, the 90 percentile distance estimation error is within 2.5cm.
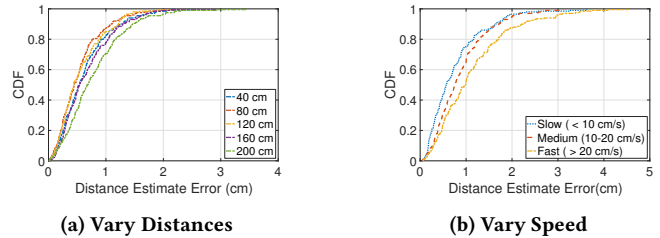

(a) Vary Distances   **(b) Vary Speed**

Figure 15: Distance Estimation Error using 2 Frequencies.

5.2.3 Estimating Azimuth and Elevation. Next, we estimate the azimuth (*i.e.*, the relative 2D angle with the antenna) and elevation (*i.e.*, the relative angle with the orthogonal plane), while keeping the other parameters the same. We change the azimuth from 20 to 160 degree (20 degree apart) and change the elevation 10 degree to 70 degree (20 degree apart), which cover 32 possible configurations. Fig. 16(a) shows that the azimuth estimation error is within 6 degree up to 2 m away when we change either the azimuth or elevation. Fig. 16(b) shows that when we change the azimuth and elevation together, our tracking achieves within 6.5 degree error at 1 m away. Fig. 16(c) and Fig. 16(d) show that both 90-percentile azimuth and elevation errors remain within 8 degree even if we vary the rotation speed at a 1m distance, validating the effectiveness of our algorithm for AoA tracking under different scenarios. As before, increasing distance and speed increases the error due to lower SNR and fewer samples during a rotation.
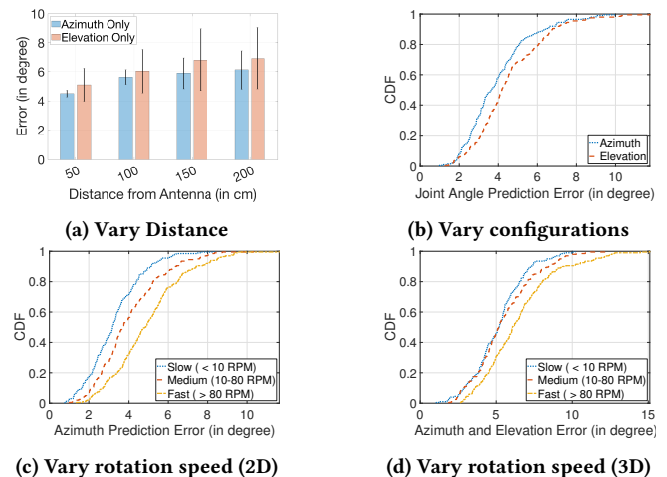

(a) Vary Distance   **(b) Vary configurations**

(c) Vary rotation speed (2D)   **(d) Vary rotation speed (3D)**

Figure 16: Azimuth & Elevation Error.

5.2.4 Estimate Moving Direction. To estimate the rotation direction, we change the rotation direction from 1m away by changing the azimuth from 20 to 160 degree (20 degree apart) with 6 different rotation axes. Using the same set of configurations, we move the

ball from 2m distance toward and away from the RFID antenna to estimate the translation. As shown in Fig. 17(a), we can estimate the direction of translation movement with almost 100% accuracy at different speeds. Moreover, Fig. 17(b) shows that we can estimate the rotation direction accurately over 95% cases at a high rotation speed. We miss some of the cases due to fewer samples and smaller change during a rotation in some configurations.
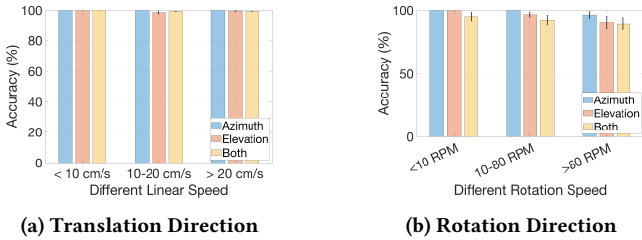

(a) Translation Direction

(b) Rotation Direction

Figure 17: Moving Direction Estimation.

5.2.5 Rotation and Translation Movement. We change the rotation speed from 5 RPM to 100 RPM and the translation movement speed from 1 cm/s to 100 cm/s. By varying the azimuth from 20 to 160 degree in 10 degree apart and the elevation from 10 to 70 degree in 10 degree apart, and the rotation axes, we generate 64 possible rotation axis configurations. As shown in Fig. 18(a), when both the rotation and translation speeds are small, the 90 percentile error is within 2cm; when both speeds increase, this error increases up to 6.5cm. Fig. 18(b) shows the 90 percentile RPM errors are around 2 and 4 for these two scenarios, respectively.
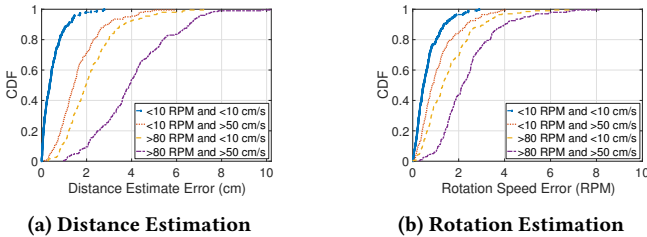

(a) Distance Estimation

(b) Rotation Estimation

Figure 18: Error in Rotation & Translation Speed Estimation.

Fig. 19 shows CDFs of the azimuth and elevation estimation error for a similar setup. As it shows, the 90 percentile estimation errors increase to 6 and 7.5 degree, respectively.
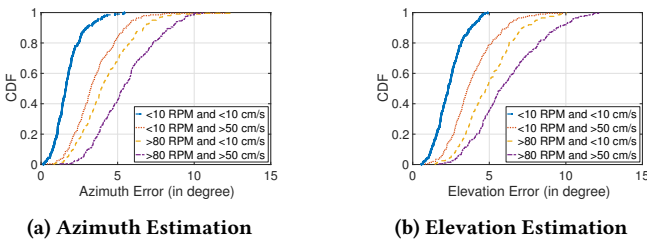

(a) Azimuth Estimation

(b) Elevation Estimation

Figure 19: Error in Azimuth & Elevation Estimation.

Furthermore, Fig. 20(a) shows the estimation error of different axes at different rotation and translation speeds. The median error of rotation axis estimation is within 5 degree and the 90 percentile error is within 7.5 degree. Fig. 20(b) further compares the estimation error using our received signal model versus a simpler model that only considers the impact of the distance as in Tagyro [36]. As we can see, our algorithm yields much lower error: the median errors is within 5 degrees in our case versus 40 degrees in the other case.
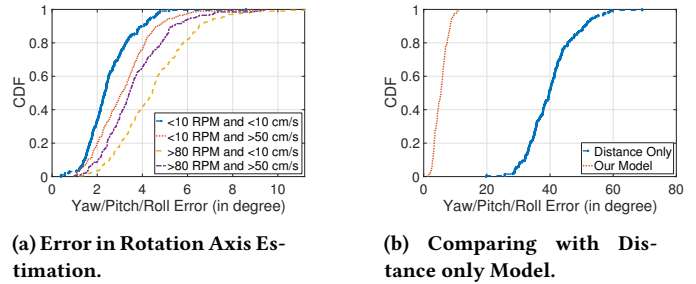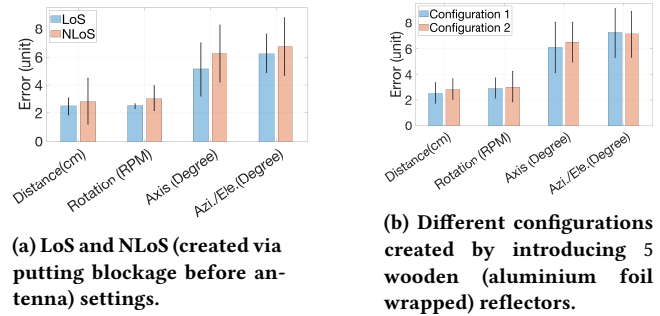

(a) Error in Rotation Axis Estimation.

(b) Comparing with Distance only Model.

Figure 20: Error in Rotation Axis Estimation.

(a) LoS and NLoS (created via putting blockage before antenna) settings.

(b) Different configurations created by introducing 5 wooden (aluminium foil wrapped) reflectors.

Figure 21: Performance in Non-line-of-sight (NLoS) setting and different static multi-path setting.

(a) Dynamic Multi-path situation is created when a user moves around.

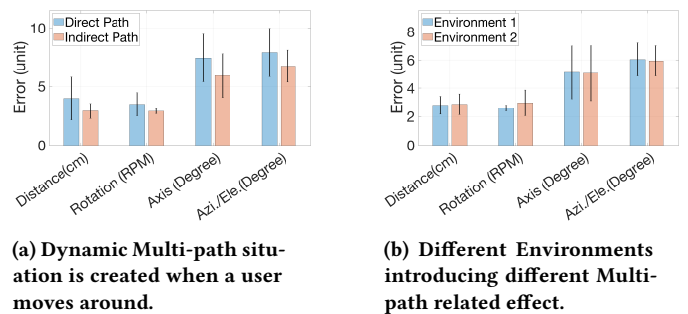**(b) Different Environments introducing different Multi-path related effect.**

Figure 22: Environment 1 and Environment 2 differ in relative locations of the furniture and desktops in the lab.

Impact of blockage and multipath: We create a blockage by putting a wooden barrier (1 m × 1m large, 5 cm thick) in front of the reader antenna. We perform a subset of the previous experiments involving both rotation and translation. Fig. 21(a) shows that error increases within 10%. Blockage does not significantly increases the error since RFID signal can penetrate through the obstacle.

Next, we introduce static multipath by placing 5 wooden reflectors wrapped with aluminum foil in the same way as the multipath experiments in Section 3.3. As shown in Fig. 21(b), the rotation axis and relative angle error are within 8 degree in both configurations. Moreover, the distance estimation and rotation speed estimation error remain small: within 3cm and 4 RPM, respectively.

To further evaluate the impact of multipath, we create dynamic multipath by moving the same wood barrier randomly between the tag and reader antenna (blocking) or near the tag and reader antenna (non-blocking). As shown in Fig. 22(a), the errors under dynamic multipath with and without blocking are 20% and 8-10% higher than in the normal setting (*i.e.*, LoS without dynamic multipath), respectively. Dynamic multipath increase errors in both cases. Blocking has higher errors due to reduced RSS. Nevertheless, the errors in both cases are low since the general trends under dynamic multipath remain similar as shown in Fig. 4(c) and (d).

We further evaluate the performance in two locations – a lab and a conference room when the calibration is performed in the lab. Fig. 22(b) shows that the errors are similar, which indicates the scheme is fairly robust to the environment change.

6 CONCLUSION

In this paper, we design a passive RFID-tag based motion sensing system for a moving ball using a single commercial-off-the-shelf antenna. To our knowledge, it is the *first* battery-free sensing system that uses a single RFID reader antenna to sense general motion. This is achieved by leveraging the polarization and non-uniform antenna gains in the passive RFID system. Our system can accurately estimate the rotation and translation motion of a moving ball. As part of our future work, we are interested in applying our approach to sports analytics.

7 ACKNOWLEDGMENTS

REFERENCES

[1] Impinj speedway uhf rfid reader. https://www.impinj.com/products/readers/, 2017. [Online] Last Accessed : 07/12/2017.

[2] Speedway revolution reader application note low level. http://bit.ly/2geiFVA, 2017. [Online] Last Accessed : 07/12/2017.

[3] 3 axis nema34 stepper motor driver. https://www.amazon.com/dp/B07DX83J46/, 2020. [Online] Last Accessed : 03/01/2020.

[4] Alien squiggle rfid white wet inlay (aln-9740, higgs-4). https://www.atlasrfidstore.com/alien-squiggle-rfid-white-wet-inlay-aln-9740-higgs-4/, 2020. [Online] Last Accessed : 03/01/2020.

[5] Arduino uno rev3. https://store.arduino.cc/usa/arduino-uno-rev3, 2020. [Online] Last Accessed : 03/01/2020.

[6] Goniometer. https://en.wikipedia.org/wiki/Goniometer, 2020. [Online] Last Accessed : 03/01/2020.

[7] High range gyroscopes. https://www.analog.com/en/products/sensors-mems/gyroscopes.html, 2020. [Online] Last Accessed : 03/01/2020.

[8] High speed belt driven linear actuator with stepper motor. https://www.fuyumotion.com/high-speed-belt-driven-linear-actuator-with-stepper-motor.html, 2020. [Online] Last Accessed : 03/01/2020.

[9] Invengo xc-af26 high gain rfid antenna. https://www.atlasrfidstore.com/invengo-xc-af26-high-gain-rfid-antenna/, 2020. [Online] Last Accessed : 03/01/2020.

[10] Linear motion system controller card for cnc machine. https://www.fuyumotion.com/linear-motion-system-controller-card-for-cnc-machine.html, 2020. [Online] Last Accessed : 03/01/2020.

[11] Nema 34 single shaft stepper motor 640 oz-in. https://www.amazon.com/Nema-Single-Shaft-Stepper-Motor/dp/B007QM5VEU, 2020. [Online] Last Accessed : 03/01/2020.

[12] Fadel Adib, Zachary Kabelac, and Dina Katabi. Multi-person localization via RF body reflections. In *Proc. of NSDI*, 2015.

[13] R. Bhattacharyya, C. Floerkemeier, and S. Sarma. Low-cost, ubiquitous rfid-tag-antenna-based sensing. *Proceedings of the IEEE*, 98(9):1593–1600, Sep. 2010.

[14] M. C. Caccami, S. Manzari, and G. Marrocco. Phase-oriented sensing by means of loaded uhf rfid tags. *IEEE Transactions on Antennas and Propagation*, 63(10):4512–4520, Oct 2015.

[15] Wei Gong and Jiangchuan Liu. Sifi: Pushing the limit of time-based wifi localization using a single commodity access point. *Proc. ACM Interact. Mob. Wearable Ubiquitous Technol.*, 2(1):10:1–10:21, 2018.

[16] Mahanth Gowda, Ashutosh Dhekne, Sheng Shen, Romit Roy Choudhury, Lei Yang, Suresh Golwalkar, and Alexander Essanian. Bringing iot to sports analytics. In *14th USENIX Symposium on Networked Systems Design and Implementation (NSDI 17)*, pages 499–513, Boston, MA, 2017.

[17] Mahanth Gowda, Ashutosh Dhekne, Sheng Shen, Romit Roy Choudhury, Sharon Xue Yang, Lei Yang, Suresh Golwalkar, and Alexander Essanian. Iot platform for sports analytics. *GetMobile: Mobile Comp. and Comm.*, 21(4):8–14, February 2018.

[18] C H. Loo, Khaled ElMahgoub, Fan Yang, Atef Elsherbeni, Darko Kajfez, Ahmed Kishk, Tamer Elsherbeni, Leena Ukkonen, Lauri Sydänheimo, Markku Kivikoski, and others . Chip impedance matching for uhf rfid tag antenna design. *Progress In Electromagnetics Research*, 81:359–370, 01 2008.

[19] C. Jiang, Y. He, S. Yang, J. Guo, and Y. Liu. 3d-omnitrack: 3d tracking with cots rfid systems. In *Proc. of IPSN*, 2019.

[20] Antonio Jiménez, Fernando Seco, C. Prieto, and Jaime Guevara. A comparison of pedestrian dead-reckoning algorithms using a low-cost mems imu. pages 37 – 42, 09 2009.

[21] Kevin King, N. Perkins, Hugh Churchill, Ryan McGinnis, Ryan Doss, and Ron Hickland. Bowling ball dynamics revealed by miniature wireless mems inertial measurement unit. *Sports Engineering*, 13:95–104, 01 2010.

[22] Manikanta Kotaru, Kiran Joshi, Dinesh Bharadia, and Sachin Katti. Spotfi: Decimeter level localization using wifi. In *Proceedings of the ACM SigComm*, pages 269–282, New York, NY, USA, 2015. ACM.

[23] Manikanta Kotaru and Sachin Katti. Position tracking for virtual reality using commodity wifi. In *Proceedings of the 10th on Wireless of the Students, by the Students, and for the Students Workshop*, S3 '18, pages 15–17, New York, NY, USA, 2018. ACM.

[24] Zhihong Luo, Qiping Zhang, Yunfei Ma, Manish Singh, and Fadel Adib. 3d backscatter localization for fine-grained robotics. In *16th USENIX Symposium on Networked Systems Design and Implementation, NSDI 2019, Boston, MA, February 26-28, 2019*, pages 765–782, 2019.

[25] Yunfei Ma, Nicholas Selby, and Fadel Adib. Minding the billions: Ultra-wideband localization for deployed rfid tags. In *Proceedings of the 23rd Annual International Conference on Mobile Computing and Networking*, MobiCom '17, pages 248–260. ACM, 2017.

[26] Yunfei Ma, Nicholas Selby, and Fadel Adib. Minding the billions: Ultra-wideband localization for deployed rfids. In *Proc. of ACM MobiCom*, 2017.

[27] S. Manzari, C. Occhiuzzi, S. Nawale, A. Catini, C. Di Natale, and G. Marrocco. Humidity sensing by polymer-loaded uhf rfid antennas. *IEEE Sensors Journal*, 12(9):2851–2858, Sep. 2012.

[28] Wenguang Mao, Jian He, and Lili Qiu. CAT: high-precision acoustic motion tracking. In *Proc. of ACM MobiCom*, 2016.

[29] Lanxin Qiu, Zhangqin Huang, Shaohua Zhang, Cheng Jing, Hao Li, and Shuyao Li. Multifrequency phase difference of arrival range measurement: Principle, implementation, and evaluation. *International Journal of Distributed Sensor Networks*, 2015.

[30] K. V. Seshagiri Rao, Pavel V. Nikitin, and Sander F. Lam. Antenna design for uhf rfid tags: A review and a practical application. *IEEE TRANS. ON ANTENNAS AND PROPAGATION*, 2005.

[31] Longfei Shangguan and Kyle Jamieson. Leveraging electromagnetic polarization in a two-antenna motion tracking system. *ACM CoNext*, 2016.

[32] Jingxian Wang, Junbo Zhang, Rajarshi Saha, Haojian Jin, and Swarun Kumar. Pushing the range limits of commercial passive rfids. In *Proc. of NSDI*, 2019.

[33] Jue Wang, Fadel Adib, Ross Knepper, Dina Katabi, and Daniela Rus. Rf-compass: Robot object manipulation using rfids. In *Proceedings of the 19th Annual International Conference on Mobile Computing & Networking*, MobiCom '13, pages 3–14, New York, NY, USA, 2013. ACM.

[34] Jue Wang, Deepak Vasisht, and Dina Katabi. RF-IDraw: virtual touch screen in the air using RF signals. In *Proc. of ACM SIGCOMM*, 2014.

[35] Teng Wei and Xinyu Zhang. mTrack: high precision passive tracking using millimeter wave radios. In *Proc. of ACM MobiCom*, 2015.

[36] Teng Wei and Xinyu Zhang. Gyro in the air: Tracking 3d orientation of batteryless internet-of-things. In *Proceedings of MobiCom*, MobiCom '16, pages 55–68, New York, NY, USA, 2016. ACM.

[37] E. Weisstein. Chinese remainder theorem. https://bit.ly/2xlV42S.

[38] Yaxiong Xie, Jie Xiong, Mo Li, and Kyle Jamieson. md-track: Leveraging multi-dimensionality for passive indoor wi-fi tracking. In *The 25th Proceedings ACM MobiCom*, pages 8:1–8:16, New York, NY, USA, 2019. ACM.